Metals and Materials International
https://doi.org/10.1007/s12540-021-00967-y

Mathematical Models to Predict Flow Stress and Dynamically Recrystallized Grain Size of Deformed AA7150-5 wt% B_4C Composite Fabricated Using Ultrasonic-Probe Assisted Stir Casting Process

R. Seetharam[1] · Pagidi Madhukar[2] · G. Yoganjaneyulu[3] · S. Kanmani Subbu[4] · M. J. Davidson[2]

Received: 20 October 2020 / Accepted: 4 January 2021
© The Korean Institute of Metals and Materials 2021

Abstract
Mathematical models are among the new approaches employed to predict the properties of any material under various conditions. Mathematical models are essential for not only understanding the material properties but also estimating the cost of design, product life, and failure criteria of the product. Therefore, in the current investigation, the hot deformation (HD) behaviour and microstructure alteration of deformed AA7150-5 wt% B_4C composite was studied through a mathematical model. The new AA7150-5 wt% B4C composite was fabricated through an ultrasonic-probe assisted (20 KHz, 1000 W) stir casting process. The hot compression test was performed on a hydraulic press for various deformation temperatures (623–773 K) and strain rates (0.01–1 s^{-1}). Based on the outcome, it is inferred that the flow stresses and microstructures of AA7150-5 wt% B_4C composite was significantly altered during the hot compression test under various deformation conditions. The constitutive and dynamically recrystallized grain (DRXed) models were developed as a function of various deformation conditions of deformed AA7150-5 wt% B_4C composite, which was then applied to forecast the flow stress and grain size behaviour for different deformation conditions. The flow stress and DRXed grain size were obtained through the proposed constitutive and DRXed models are correlated with experimental results, with excellent accuracy. The models developed are reliable to predict the AA7150-5 wt% B_4C properties for various conditions.

Keywords DRX modeling · Constitutive equation · Grain size · Ultrasonication · Hot compression test

1 Introduction

Industries are always in search of new types of materials for structural applications with higher material properties like thermal, wear, and mechanical along with ease of manufacturing process reach the desired properties [1]. The characteristics like ultralight-weight, very high porosity, high compression, high energy absorption, and high strength with low thermal conductivity make these materials ideal for structural applications in marine industry, aerospace, military and automobile applications [2–4].

Ceramic micro-particles are mixed into the Aluminum (Al) alloys to improve its moderate material properties like hardness, ductile, strength, wear and other properties [5]. Since a couple of years, micro-particulates have been proposed to manufacture Metal Matrix Composites (MMC) and these evidence far better material properties when the particulates attain uniform distribution [6], as has been proved by experiments and mentioned in the literature by several researchers, particularly with respect to strength,

✉ R. Seetharam
seetharam@iiitdmj.ac.in

Pagidi Madhukar
pmadhu88@gmail.com

G. Yoganjaneyulu
yogi.08390@gmail.com

S. Kanmani Subbu
sksubbu@iitpkd.ac.in

M. J. Davidson
mjdavidson2001@yahoo.co.in

[1] Department of Mechanical Engineering, PDPM Indian Institute of Information Technology, Design and Manufacturing, Jabalpur 482005, India

[2] National Institute of Technology, Warangal, Telangana 506004, India

[3] Vignan's Institute of Information Technology, Visakhapatnam, Andhra Pradesh, India

[4] Indian Institute of Technology, Palakkad, Kerala 678557, India

Published online: 27 May 2021

density, hardness, wear and corrosion resistance, coupled with fatigue life and high temperature creep resistance of the material [7–9]. Al-Zn-Mg-Cu alloys composites are lightweight, have high strength and stiffness for military, aerospace and automobile applications [10]. Several fabrication methods are available to prepare MMCs. Among them, liquid metallurgy method via stir casting route has proved to be a potential method for distribution of fine particles with high production capability and low cost [11, 12]. Ultrasonic vibration assisted stir casting technique is one of the best approaches for refinement of composites, degassing as well as purifying molten liquid Al at the microscopic level, and ensuring homogeneous distribution of particulates [13, 14].

Dynamic Recrystallization (DRX) plays a major role in determining the material properties of monolithic substances and their composite materials. The grain refinement of the materials is attained during hot deformation process due to DRX phenomena by initiating the nucleation in the deformed materials [15]. DRX can be achieved through different mechanisms like adding particulates into the matrix alloy [16], changing the deformation conditions (strain rate and temperature) [17] as well as degree of deformation [18]. The behaviour of DRX can be greatly affected by particle reinforcement during the hot deformation process of MMCs [19–22] due to the hard and brittle in nature.

There have been numerous researches on Al7150 alloys to study the hot deformation and microstructural behaviour under various conditions and processes [10, 23–27]. However, only limited literature is available on DRX behaviour of Al7150 alloy with ceramic reinforcement during the compression test. Among all the ceramic reinforcements, B_4C has superior properties such as lower density (2.52 g/cc) [28] and higher hardness (2900–3580 kg/mm^2) [29] because of which it offers high strength to low weight ratio. The idea is to demonstrate the DRX behaviour of B_4C particle reinforced composites because of their potential applications in aerospace, automobile, defence and nuclear industries [30, 31]. In nuclear reactors, the heavy nucleus releases a high amount of energy as well as several free neutrons due to continuous nuclear fission. Therefore, neutron moderators/control rods are mandatory with high neutron absorption rate to control the continuous reaction. B_4C shows high neutron absorption property and B_4C reinforced composites can be used as a fuel storage tank material of nuclear reactor. Hence, it is necessary to analyse the microstructure as well as DRX behaviour of B_4C ceramic particulate reinforced composite at different deformation parameters for ensuring better properties of the composite. The constitutive and microstructure models are to be developed for an alloy and its composites to estimate the microstructural and deformation behaviour of the material.

The main objective of the present research is to realize the fundamentals of particulate reinforced Al7150 composites during the hot deformation and its thermo-mechanical parameters effects on structural changes of composite materials and flow stress.

2 Materials and Methodology

The matrix material selected was Al7150, with B_4C as reinforcement. Al7150 alloy ingots were purchased from " Venuka Engineering Private Limited, Hyderabad" with a chemical composition of Al-2.56 Mg-6.37Zn-2.25Cu-0.08Si-0.009Mn-0.12Fe-0.11Zr (mass%), density 2.83 g/cc, > 99% purity and B_4C from "Supertek Dies, Delhi, India" with the average particle size of 45 µm, density 2.52, > 99.9% purity as shown in Fig. 1.

The B_4C reinforced composite was fabricated though ultrasonic assisted stir casting process (melting, particulates mixing, stirring, ultrasonication). In short, this fabrication process involves a combination of ultrasonic vibration and stir casting methods. Stir casting method was used to mix the ceramic particulates with ceramic coated rotary impeller and the process was performed at 750 °C (above liquidus) temperature to allow the spread of ceramic particulates due to low viscosity and high flowability of liquid property. Ultrasonication was also conducted at the same liquidus temperature, where the ultrasonication energy waves spread throughout liquid pool effectively, leading to the creation of high-pressure bubbles and acoustic stream. The combined effect of these processes encourages homogeneous distribution of fine ceramic particulates. The schematic diagram of the ultrasonic assisted stir casting process is shown in Fig. 2. The homogeneously dispersed melt was poured into

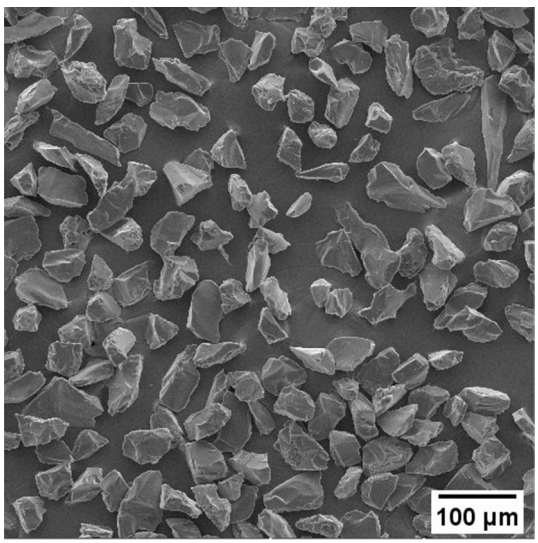

Fig. 1 Initial scanning electronic microscopic morphology of Boron Carbide particles

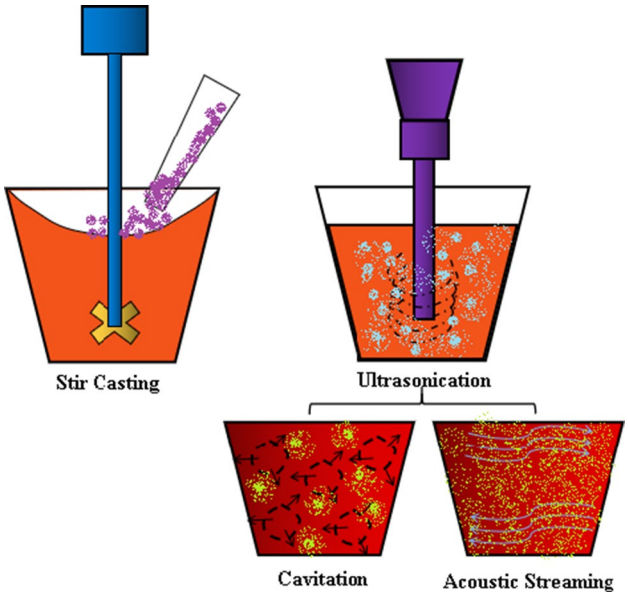

Fig. 2 Schematic diagram of the ultrasonic vibrated stir casting process

preheated (450 °C) mould of 10 mm holes and allowed to cool at atmospheric temperature. Machining was preformed to get the required shapes (1.5 aspect ratio i.e., ø6 mm and 9 mm length) for compression test.

The hot compression test on Al7150-B_4C composites at different strain rates (0.01, 0.1 and 1 s^{-1}) as well as deformation temperatures (623, 673, 723 and 773 K) was carried on a hydraulic press (Schematic Fig. 3). Two thermo-couples were used to measure deformation temperature in which one thermocouple was placed near the specimen to measure the specimen temperature and the other one inside the furnace to measure the furnace temperature. Both specimen and furnace temperatures were controlled within the range of ± 5 °C. During the experiment, the test specimens were soaked at a test temperature for 30 min to get evenly distribute of temperature throughout the test specimens and then incremental compression loads applied till to reach a total true strain of 0.6. After getting required strain the specimen was instantly quenched in water to get uniform microstructure in the composite. The displacement and load values were noted from the hydraulic press data logger unit. Figure 4 demonstrates the experimental procedure and microstructure evolution process under different conditions.

Optical Microstructure (OM) was used to analyse the grain structures of the hot deformed Al7150-B4C composite samples at different deformation conditions and these samples were prepared through parallel sectioning (compression axis along the centreline) of the tested Al7150-B_4C composite samples. All the sectioned sample surfaces were manually polished as per standard procedure and then etched for 60 s in Keller's liquid solution. The grain size of hot deformed Al7150-B_4C composites was measured for different deformation conditions through "Line Intercept Method (LIM)".

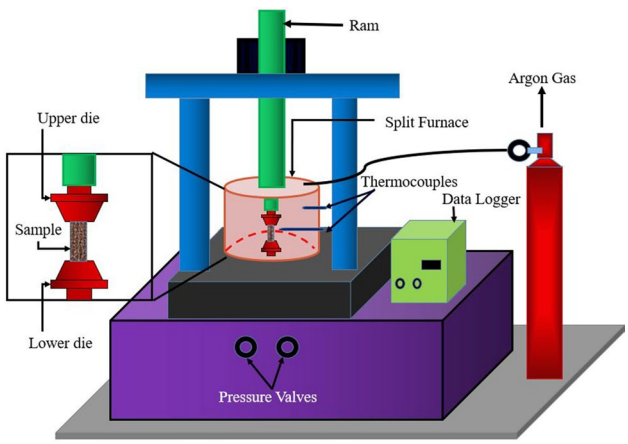

Fig. 3 Schematic diagram of hydraulic press

3 Results and Discussion

3.1 Study of Flow Stress Behaviour

Figure 5 demonstrates the hot deformation behaviour of deformed AA7150-5 wt% B_4C composite for various deformation temperatures (623–773 K) and strain rates

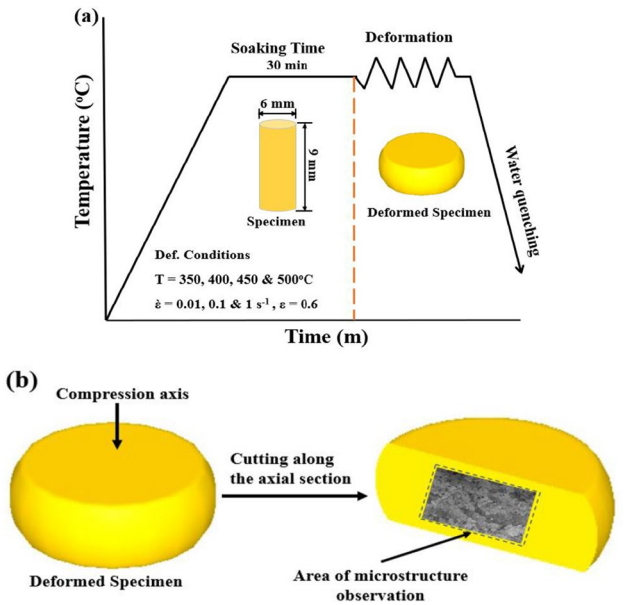

Fig. 4 **a** Schematic diagram of experimental procedure at different deformation conditions; **b** microstructure evolution area

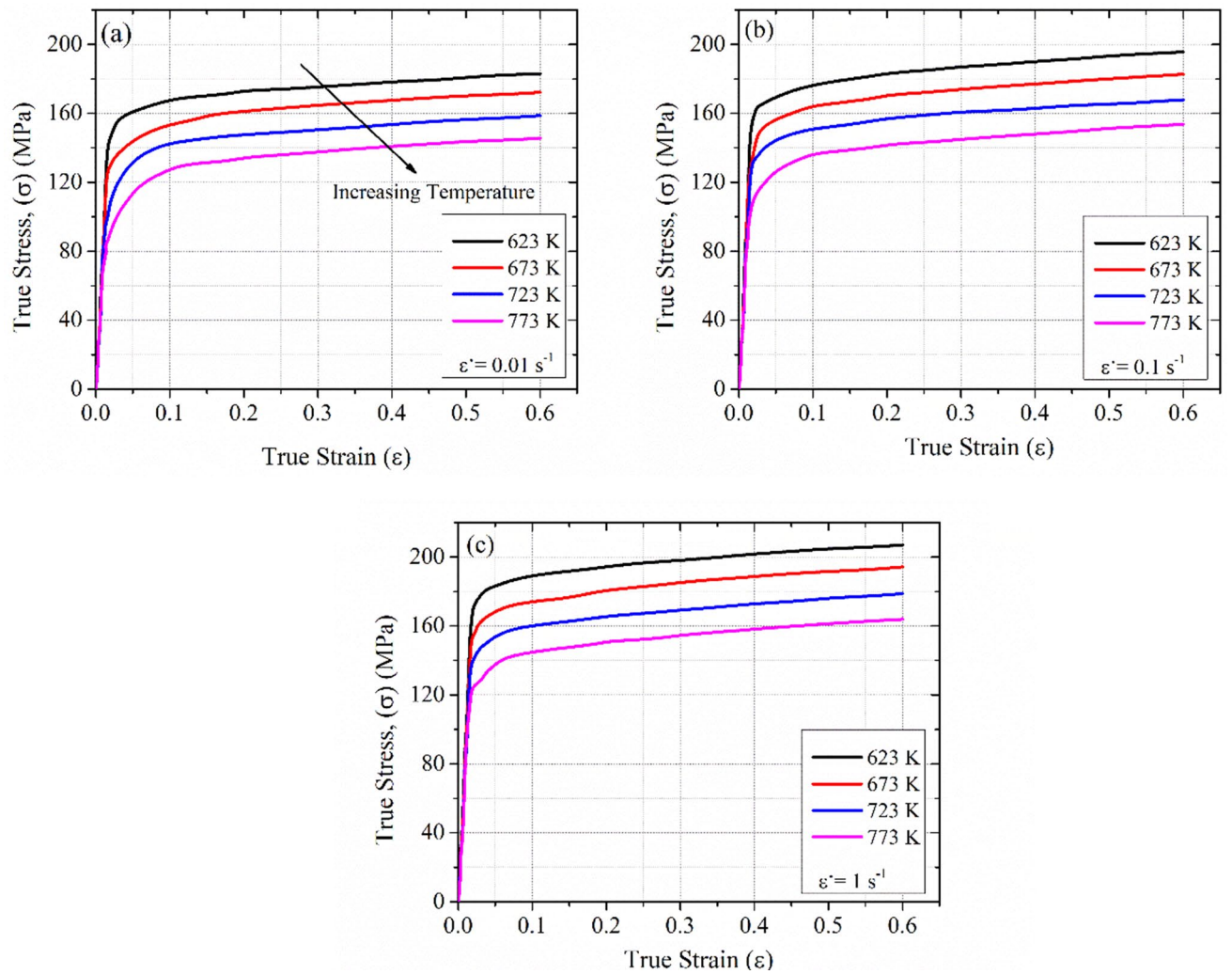

Fig. 5 True stress-true strain plots for different temperatures and strain rates of **a** 0.01 s^{-1}; **b** 0.1 $s^{-1}$and **c** 1 s^{-1}

(0.01–1 s^{-1}). It is described that the hot flow curves are significantly influenced by different HD conditions.

The deformation curves lower with higher temperature and with lowering strain rate. There is decrease in flow stress with an increase in deformation temperature because of thermal softening in the composite; that means the resistance to dislocation motion decreased as it promotes reduction in flow stress. On the contrary, as the temperature increases, the DRX grains are amplified thereby increasing the dislocation motion, which decreases the flow stress [32]. The flow stress values are higher with increasing strain rates during the compression test, the underlying reason being that the dislocation density is significantly enlarged and dislocations are tangled with higher strain rate [33, 34]. Further, it is observed that in the beginning of the stress- strain curves, flow stress quickly increased with higher strain values because work hardening assumes a leading role at lower strain values. The dislocation density is improved substantially due to reduction of porosity at initial deformation loads and lower strain values. At certain strain values, the work hardening and softening mechanism are dynamically balanced due to which the flow curves exhibited peak value. At higher strain values, flow stress decreased and becomes stable up to the end of deformation, indicating DRX phenomenon. With increasing strain values, work hardening starts to decrease and this causes stability as a result stress-strain curves becoming flat at higher strain values.

3.2 Microstructures Analysis

Figure 6 illustrates the optical microstructures of AA7150-5 wt% B_4C composite prior to the compression test. Figure 6a demonstrates the dispersion of B_4C reinforcement in AA7150 matrix and it is assumed that the reinforcement is homogeneously distributed all over the matrix with equal distance between the particles. Figure 6b represents

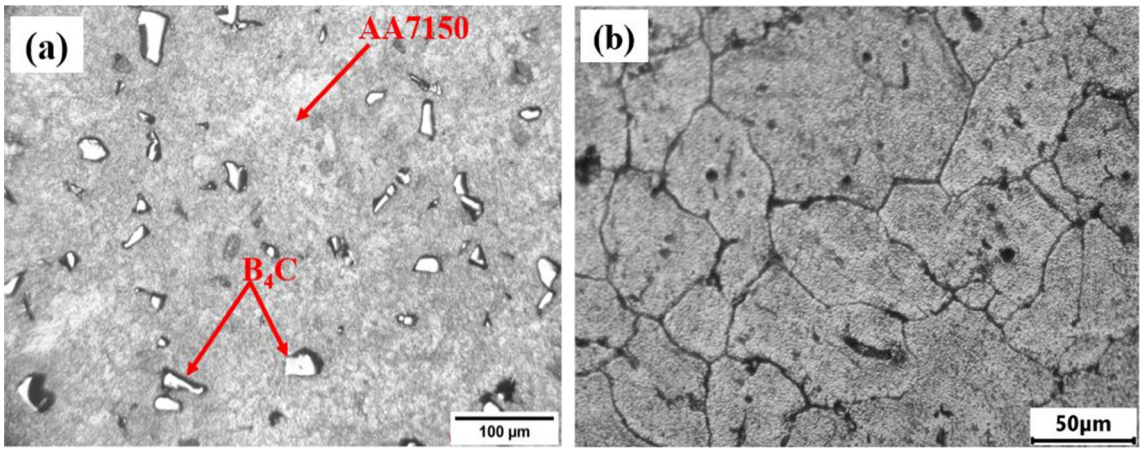

Fig. 6 Microstructures of AA7150-5 wt% B_4C composite is **a** distribution of B_4C reinforcement and **b** initial grains structures of AA7150-5 wt% B_4C

the microstructure of AA7150-5 wt% B_4C composite prior to the compression test. It is seen that the grains are equiaxed with average grain size of 51 ± 2 µm obtained from casting. The grains are altered and elongated perpendicular to the compression direction after compression test.

The grain size of the deformed AA7150-5 wt% B_4C composite was measured for different deformation conditions such as temperature and strain rate and it was found to vary from 3 to 48 µm. Figure 7 depicts the microstructure of deformed AA7150-5 wt% B_4C composite for various deformation temperatures according to the strain rate of 0.01 s^{-1}. It is noticed from the microstructure the preliminary grains are plastically elongated and formed new small irregular grains is known as dynamically recrystallized grain (DRXed). The average DRXed size was determined for different temperatures of 623, 673,723 and 773 K are 13.15, 17.37, 21.32 and 26.18 µm, respectively, corresponding to the strain rate of 0.01 s^{-1} as shown in Fig. 9a. The above results indicate that the DRXed grain size grownup with higher temperature. The underlying reason is that the grain growth rate increased with increasing temperature, since diffusion rate among the particles was amplified and it facilitates growth in grain size [35, 36]. Figure 8 illustrates the microstructure for various strain rates of 0.01–1 s^{-1} at the temperature of 773 K of deformed AA7150-5 wt% B_4C composite. It is noticed that the original grains were entirely changed, and it forms new fine DRX grains during the compression test. The average DRXed grain size measured for various strain rates of 0.01, 0.1 and 1 s^{-1} were 26.18, 23.05, and 19.46 µm, respectively as shown in Fig. 9b. It confirms that the DRXed grain sizes are reduced with higher strain rate for the corresponding temperature. The dynamic recovery rate is lower at higher strain rate because of which the nucleation rate stimulated the deformed structure for a given deformation temperature [16, 37, 38]. Moreover, it was observed from the deformed microstructures that the grain boundaries were surrounded by reinforcement particles, which promote the DRX in the matrix irrespective of deformation conditions [39]. Therefore, due to DRX behaviour in deformed structures, very fine microstructures were obtained which promote good mechanical properties.

3.3 Constitutive Analysis

In general, constitutive models are applied to estimate the hot deformation behaviour of any material and to build the correlation between deformation conditions and the flow stress of the materials [40]. The hyperbolic-sine function demonstrates the correlation between flow stress, strain rate, and temperature across a wide range of stresses and was proposed by Sellars and McTegart [41] as follows.

$$\varepsilon' = A[\sinh(\alpha\sigma)]^n exp\left(-Q/RT\right) \tag{1}$$

where $\acute{\varepsilon}$ is strain rate in s^{-1}, σ is flow stress in MPa, Q is activation energy in KJ mol^{-1}, R is universal gas constant (8.314 J mol^{-1} K^{-1}), T is deformation temperature in Kelvin (K), A and n are material constants, and α is stress multiplier.

Based on the different stress levels the Sellars and McTegart can be rewritten as:

$$\varepsilon' = A_2 \exp(\beta\sigma) \exp\left(Q/RT\right) \quad [\alpha\sigma > 1.2] \tag{2}$$

$$\varepsilon' = A_2 \left[\exp(\beta\sigma)\right] exp\left(-Q/RT\right) \quad [\alpha\sigma > 1.2] \tag{3}$$

$$\varepsilon' = A[\sinh(\alpha\sigma)]^n \exp\left(-Q/RT\right) \quad [\alpha\sigma \text{ for any values}] \tag{4}$$

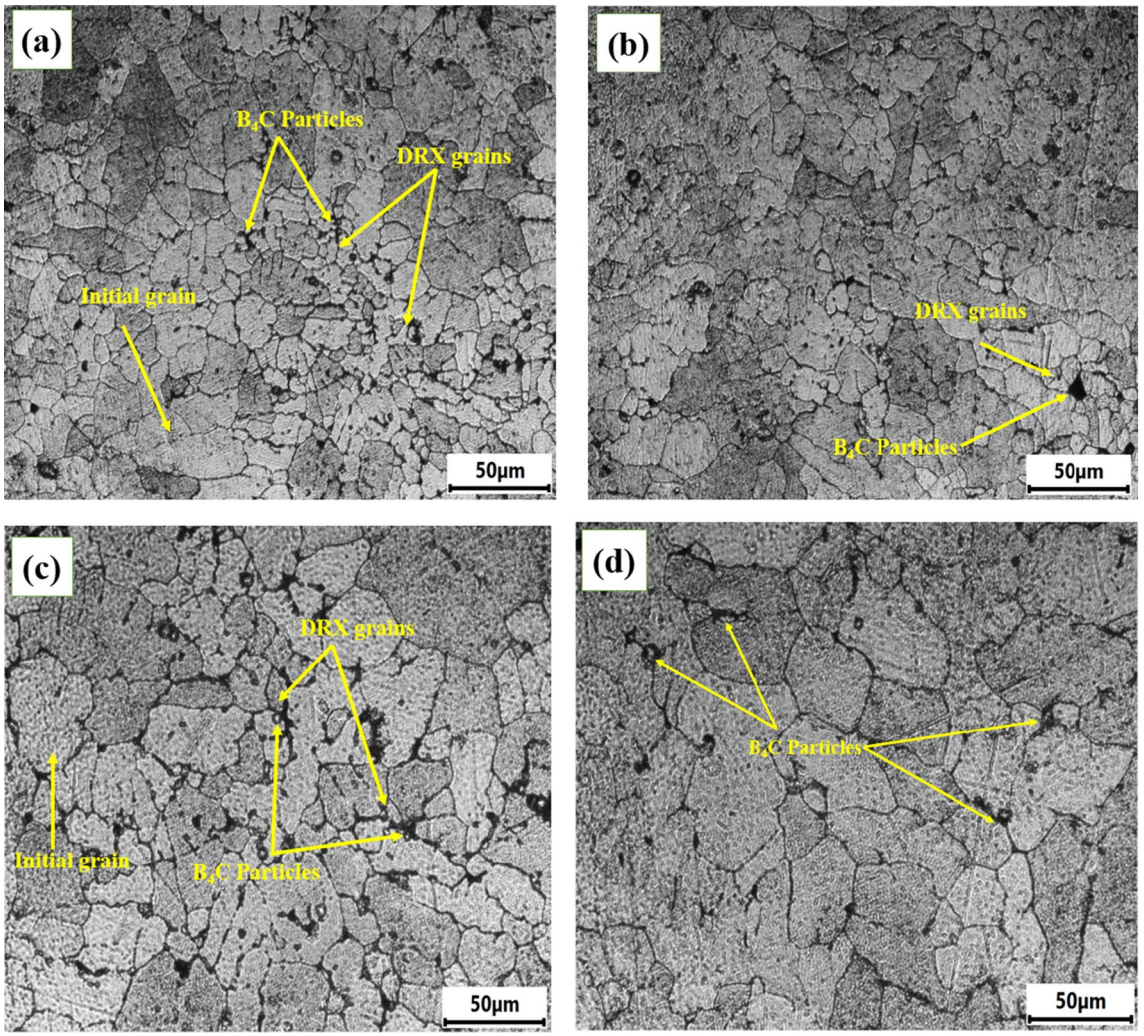

Fig. 7 Microstructures of deformed AA7150-5 wt% B_4C composite at 0.01 strain rate for various temperatures are **a** 623 K; **b** 673 K; **c** 723 K and **d** 773 K

where, $A_1 = A\alpha^n$, $A_2 = A/2^n$, and $\alpha = \beta/n$ are constants and it can be obtained from the experimental results. Eq. (2) represents the power law that can be applied for low level stress values, Eq. (3) indicates the exponential law to be used for high level stress values; however, the hyperbolic sine law of Eq. (4) is appropriate for all levels of stress values.

It is possible to study the combine effects of deformation conditions (strain rate and temperature) on flow stress through the Zener–Holloman parameters (Z) [42]:

$$Z = \varepsilon' \exp\left(Q/RT\right) \tag{5}$$

From the Eqs. (4) and (5) it can be written

$$Z = A[\sinh(\alpha\sigma)]^n \tag{6}$$

Furthermore, the flow stress (σ) is possible to obtain in terms of materials constants and Z parameter by applying hyperbolic sine rule to the Eq. (6).

$$\sigma = \frac{1}{\alpha}\ln\left\{\left(\frac{Z}{A}\right)^{\frac{1}{n}} + \left[\left(\frac{Z}{A}\right)^{\frac{2}{n}} + 1\right]^{\frac{1}{2}}\right\} \tag{7}$$

3.3.1 Calculation of Materials Constant n and β

To determine the material constants such as n and β, peak flow stress could be used corresponding to temperatures and strain rates. By simplifying Eqs. (2) and (3), the following expression were obtained are used to produce the materials constants n and β.

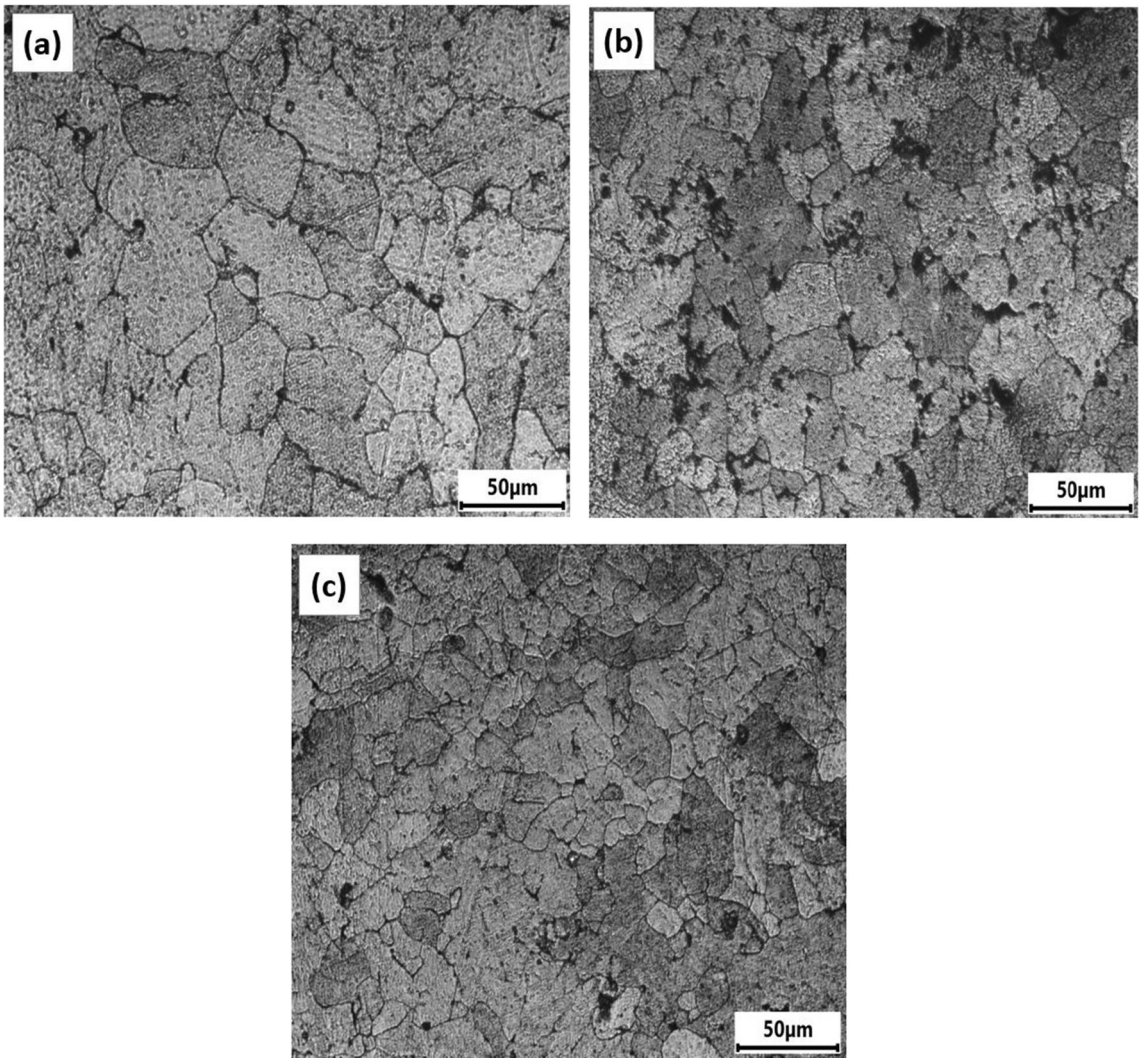

Fig. 8 Microstructures of deformed AA7150-5 wt% B_4C composite at 773 K deformation temperature for different strain rates are **a** 0.01 s^{-1}; **b** 0.1 s^{-1} and **c** 1 s^{-1}

$$\ln \varepsilon' = \ln A_1 + n \ln \sigma - \frac{Q}{RT} \tag{8}$$

$$\ln \varepsilon' = \ln A_2 + \beta \sigma - \frac{Q}{RT} \tag{9}$$

The compression test was carried out at constant temperature; hence, the above equations were re-simplified by applying partial differentiation equations:

$$n = \left[\frac{\partial ln\varepsilon'}{\partial ln\sigma}\right]_{T=const} \tag{10}$$

$$\beta = \left[\frac{\partial ln\varepsilon'}{\partial \sigma}\right]_{T=const} \tag{11}$$

Then, n and β values were determined from the Eqs. (10) and (11) by introducing flow stress and given strain rates for various deformation temperatures. Figure 10 plots demonstrating the correlation between lnέ vs. lnσ, and lnέ vs. σ for acquiring the n and β values at a true strain of 0.6. The slop of lines lnέ and lnσ, and lnέ and σ provides the n and β values respectively for different conditions. Further, α = β/n value was determined. Eq. (2) is ignored the effect of strain levels on the materials constants, which does not influence stress under steady state condition. However, at the lower strain values, the flow stress varies over a wide range which exhibits various n and β values. In compression test, strain is most significant element which influences the properties of materials such as work hardening and dynamic softening behaviour. Therefore, the effect of strain needs to be considered to establish any comprehensive constitutive model [43]. In

view of this, the material constants were determined in the strain range of 0.1–0.6 in the interval of 0.1 as described in the above procedure. The n and β values are tabulated in Table 1 for different strain levels. It is noticed from Table 1 that with increasing strain levels, the α values decreased until 0.4 strain, after which it remained the same and became independent of strain.

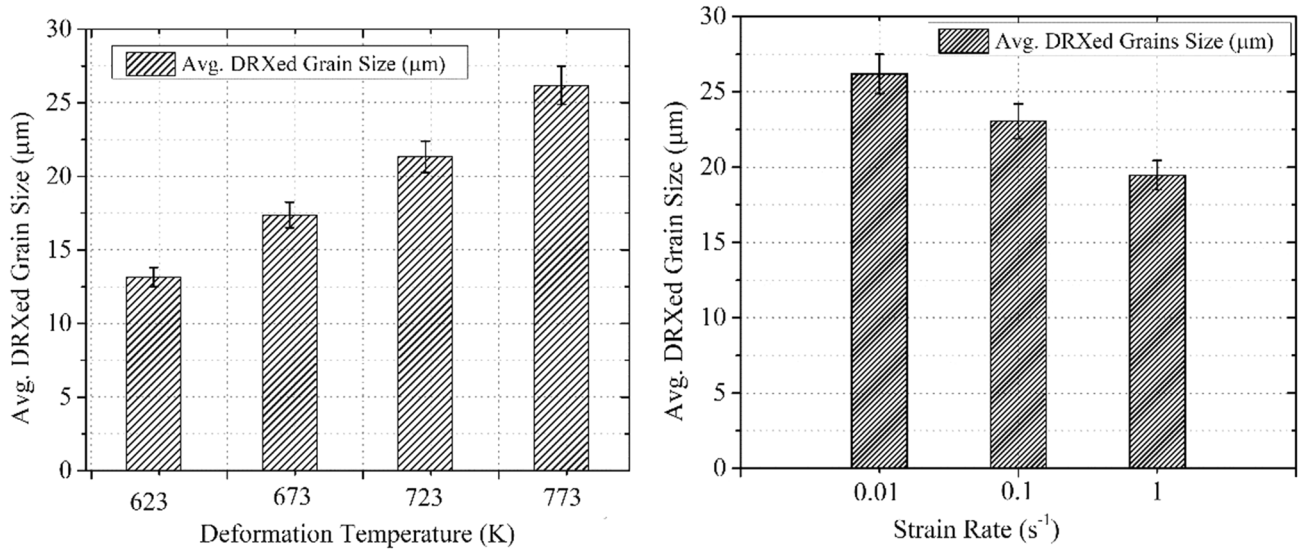

Fig. 9 Correlation between **a** deformation temperature and avg. DRXed grain size and **b** strain rate and avg. DRXed grain size of deformed AA7150-5 wt% B_4C composite

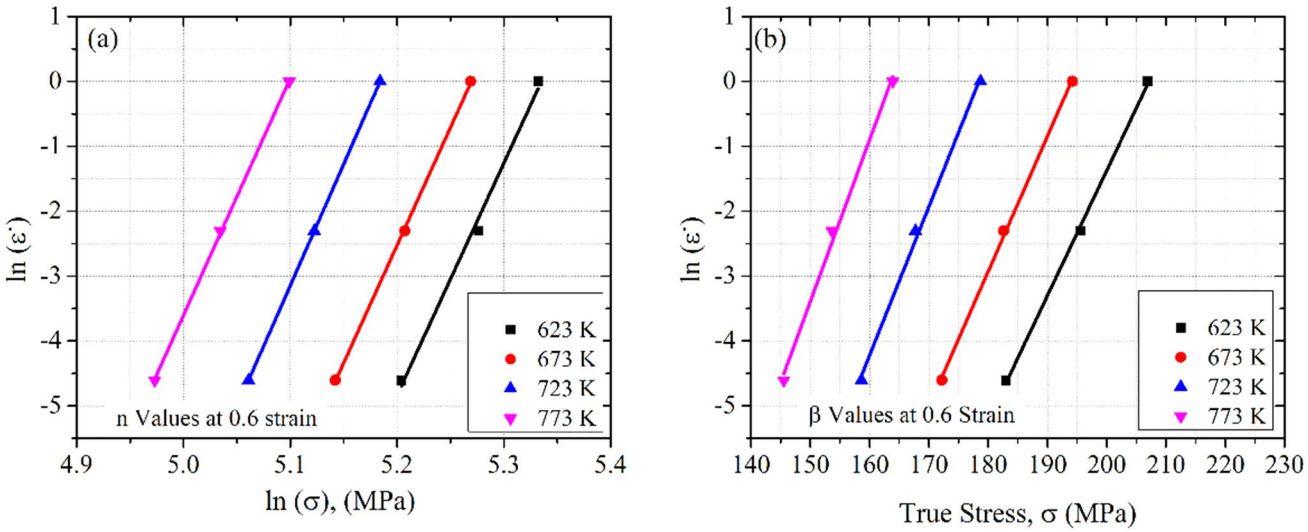

Fig. 10 Graphs for the obtaining material constant n and β values are **a** ln (σ) vs. ln (ε̇) and **b** σ vs. ln (ε̇) for various deformation temperatures

Table 1 Material constants (n, β and α) values of deformed AA7150-5 wt% B_4C composite for various true strain levels

Material constants	Strain levels					
	0.1	0.2	0.3	0.4	0.5	0.6
n	40.18	39.06	38.56	38.06	37.37	36.2
β	0.263	0.252	0.245	0.24	0.235	0.228
$\alpha = \beta / n$	0.00654	0.00645	0.00636	0.0063	0.00629	0.00629

3.3.2 Computations of Activation Energy (Q) and Z Parameters

The product of ασ values was calculated in Eq. (4) for different conditions in Table 2. It is noticed that the variations in ασ values are not applicable for either power law or exponential law of deformation behaviour for low and high stress levels. In contrast, the hyperbolic-sine is an appropriate function for a wide range of stress levels (ασ) supporting the values tabulated in Table 2. Therefore, the Q parameter can be determined with the help of hyperbolic sine function for various true strain levels, strain rates, and deformation temperatures.Equation (12) obtained from the Eq. (4) by applying the natural logarithm on both sides which gives:

$$\ln \varepsilon' = \ln A + n \ln [\sinh (\alpha\sigma)] - \frac{Q}{RT} \tag{12}$$

The compression test was done at a given constant strain rate and the partial differentiation applying to the Eq. (12) gives the expression as:

$$Q = R\left\{ \frac{\partial \ln \varepsilon'}{\partial \ln [\sinh (\alpha\sigma)]} \right\}_{T=const} \left\{ \frac{\partial \ln [\sinh (\alpha\sigma)]}{\partial \left(\frac{1}{T}\right)} \right\}_{\varepsilon'=const} \tag{13}$$

The activation energy has been calculated by introducing σ, α and the recorded temperature at a given strain rate in Eq. (13), which gives the correlation of lnέ vs. ln[sinh(ασ)] and ln[sinh(ασ)] vs. 1/T. Figure 11 plots the

Table 2 According Eqs. (3) and (4), (ασ) values are varies with various deformation conditions

Temp. (K)	Strain rate (s^{-1})	Strain levels					
		0.1	0.2	0.3	0.4	0.5	0.6
623	0.01	1.11	1.11	1.11	1.12	1.14	1.15
623	0.1	1.17	1.18	1.19	1.19	1.22	1.23
623	1	1.24	1.25	1.26	1.26	1.29	1.3
673	0.01	1.02	1.04	1.05	1.05	1.07	1.08
673	0.1	1.08	1.10	1.11	1.11	1.13	1.15
673	1	1.15	1.16	1.18	1.18	1.21	1.22
723	0.01	0.94	0.95	0.96	0.96	0.99	1
723	0.1	0.99	1.01	1.02	1.02	1.04	1.06
723	1	1.05	1.06	1.08	1.09	1.11	1.13
773	0.01	0.85	0.86	0.88	0.88	0.91	0.92
773	0.1	0.9	0.91	0.92	0.93	0.95	0.97
773	1	0.95	0.97	0.98	0.99	1.02	1.03

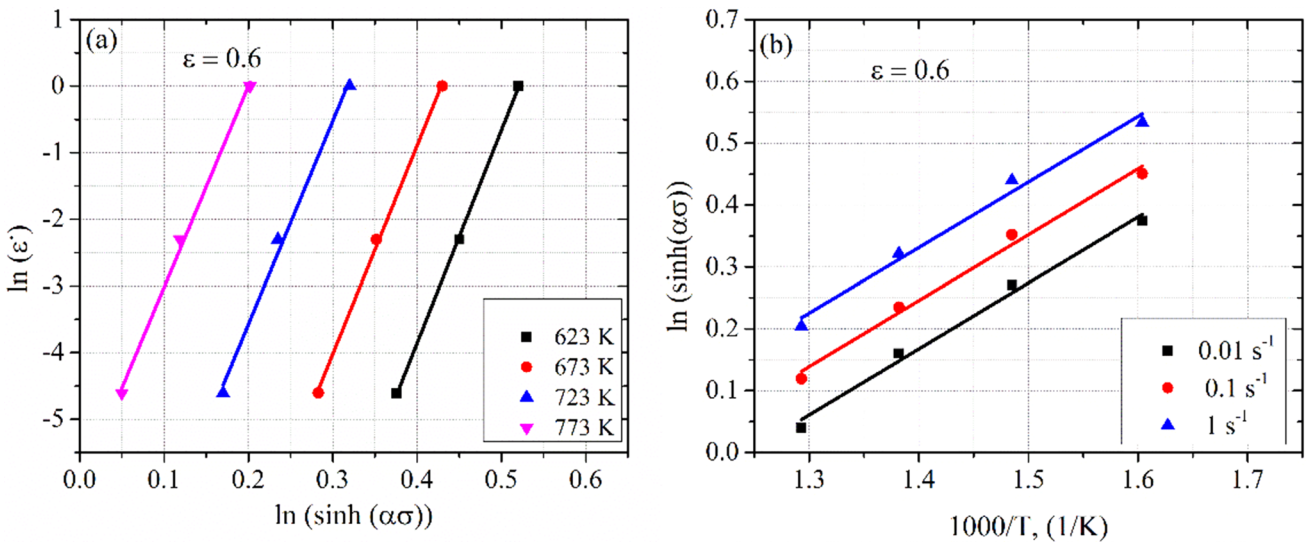

Fig. 11 Plots for the obtaining activation energy (Q) kJ/Mol. are **a** ln (sinh(ασ)) vs. ln (ε̇) and **b** 1/T vs. ln (sinh(ασ)) for different conditions

Table 3 Activation energy and material constant lnA values for various strain levels

	True strain levels						
	0.1	0.2	0.3	0.4	0.5	0.6	Average
Q (kJ/Mol)	298.45	293	284.7	279.16	275.27	274.27	284.14
lnA	41.08	39.96	38.94	37.5	36.01	34.66	38.02

Table 4 Activation energy of AA7150 alloys and composite for different conditions

Materials and conditions	Activation energy (Q), kJ/mol	References
AA7150-5 wt% B_4C composite	284.1	Present Investigation
Aged AA7150 alloy	158.8–161.4	23
Homogenized AA7150 alloy	229.75	24
Pure AA7150 alloy	227	25
Pure AA7150 alloy	229.75	28
Pure Aluminium	144.3	46

correlation between lné and ln[sinh(ασ)], and ln[sinh(ασ)] and 1/T for finding the Q parameter at a true strain of 0.6. The slope of lines lné and ln[sinh(ασ)] and, ln[sinh(ασ)] and 1/T gives Q values for different deformation conditions. Similarly, the Q parameter values are determined for various true strain levels and shown in Table 3. It is observed that the activation energy (284.1 kJ/Mol) of the deformed AA7150-5 wt% B_4C composite is higher than that of AA7150 alloys reported elsewhere, as shown in Table 4. However, the Q values of deformed AA7150-5 wt% B_4C composite is far beyond that of the self–diffusion of pure aluminum (144.3 KJ/mol) [44]. The activation energy of deformed AA7150-5 wt% B_4C composite exceeds that of pure AA7150 alloys because B_4C acts as a barrier to the plastic deformation in the alloys.

For calculating lnA values, Eq. (6) is modified by applying natural logarithm, and expressed as follows

$$\ln Z = \ln A + n\ln[\sinh(\alpha\sigma)] \tag{14}$$

Figure 12 demonstrates the correlation between ln (sinh(ασ)) and ln Z at strain levels of 0.1 and 0.6 for obtaining material constant lnA. The intercept of the lines lnZ vs. ln[sinh(ασ)] gives the lnA values for different strain levels of 0.1–0.6, as tabulated in Table 3.

The mathematical models were established between material constants and various strain levels of deformed AA7150-5 wt% B_4C composite by fitting 5th order polynomial functions as shown Fig. 13. Hence, the constitutive models developed for deformed AA7150-5 wt% B_4C composite is expressed in Eq. (15) and the coefficient of polynomial fits in Table 5. These proposed constitutive models could be useful to forecast the flow stress of deformed AA7150-5 wt% B_4C composite for various strain levels by using flow stress Eq. (7).

$$\beta = b_o + b_1\epsilon + b_2\epsilon^2 + b_3\epsilon^3 + b_4\epsilon^4 + b_5\epsilon^5 \text{ (i)}$$
$$n = c_o + c_1\epsilon + c_2\epsilon^2 + c_3\epsilon^3 + c_4\epsilon^4 + c\epsilon^5 \text{ (ii)}$$
$$\alpha = d_o + d_1\epsilon + d_2\epsilon^2 + d_3\epsilon^3 + d_4\epsilon^4 + d_5\epsilon^5 \text{ (iii)} \tag{15}$$

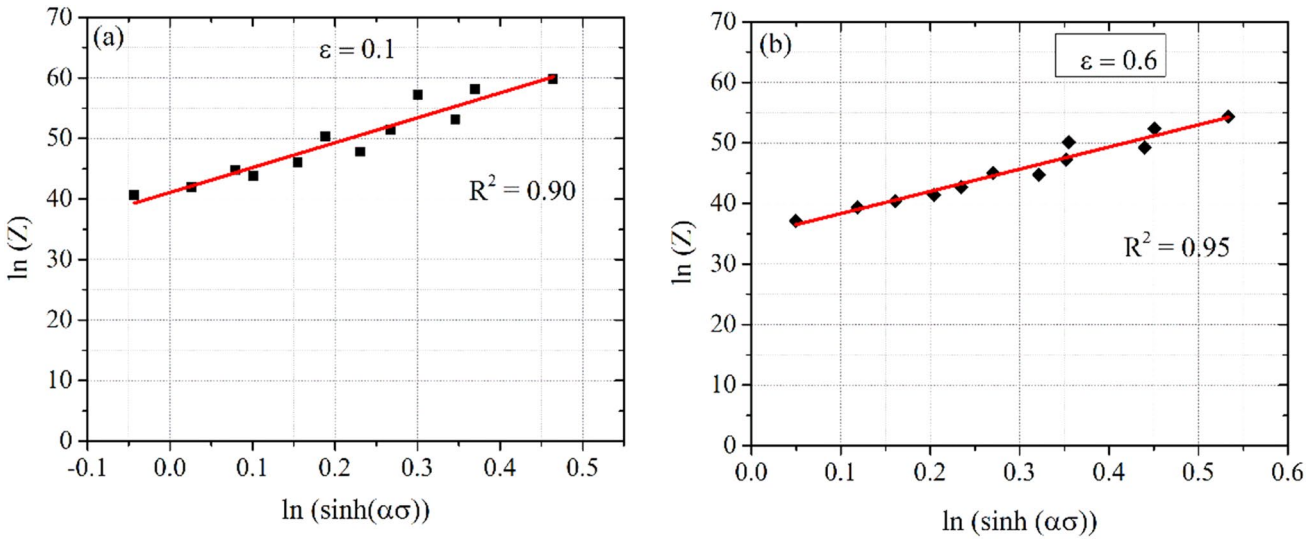

Fig. 12 Correlation between ln (sinh(ασ)) and ln Z for different strain levels of **a** 0.1 and **b** 0.6 for obtaining material constant lnA

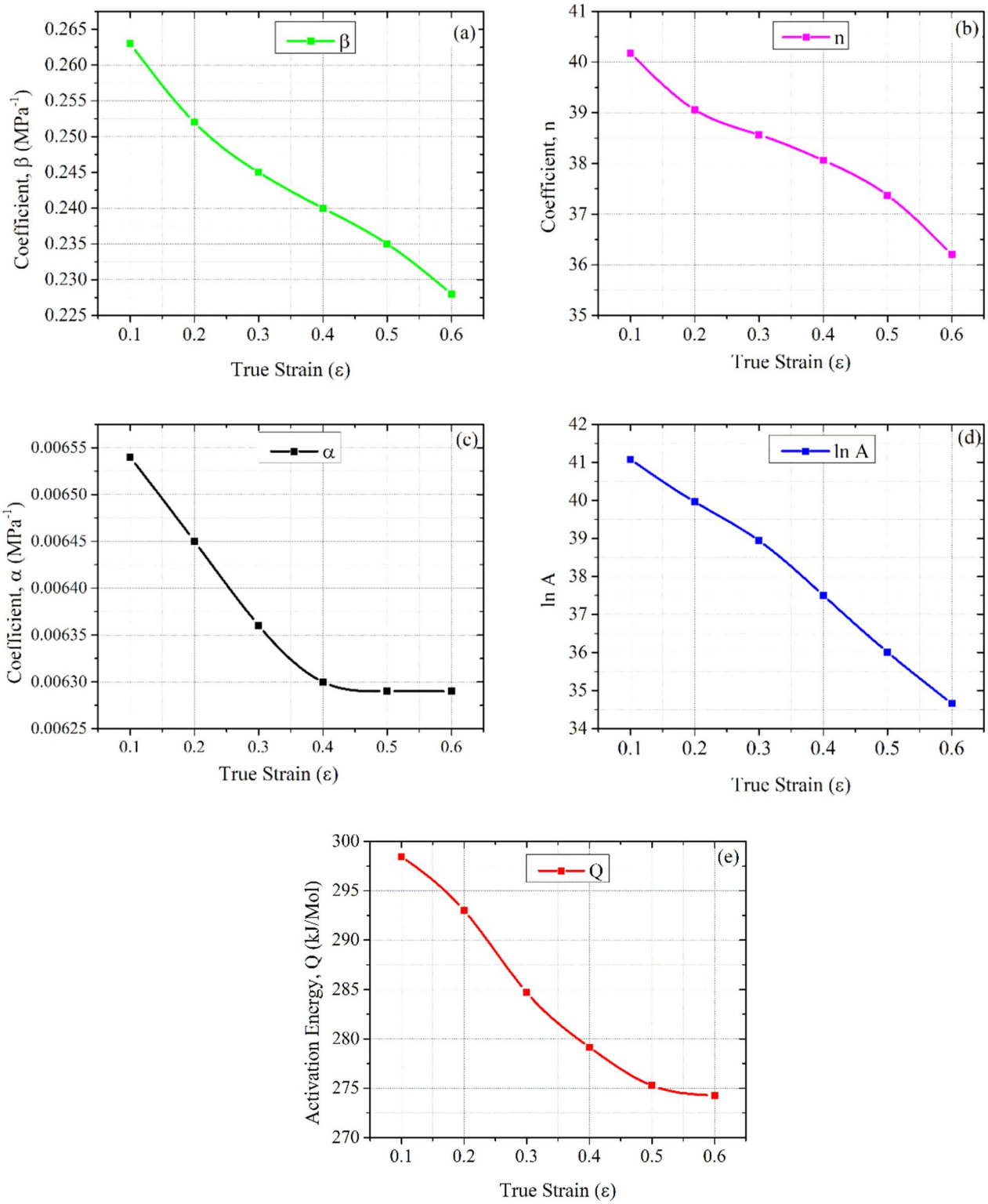

Fig. 13 Correlation between different strain levels and material constants are **a** β; **b** n; **c** α; **d** lnA and **e** Q

$$\ln A = e_o + e_1\epsilon + e_2\epsilon^2 + e_3\epsilon^3 + e_4\epsilon^4 + e_5\epsilon^5 \text{ (iv)}$$
$$Q = f_o + f_1\epsilon + f_2\epsilon^2 + f_3\epsilon^3 + f_4\epsilon^4 + f_5\epsilon^5 \text{ (v)}$$

Table 5 Coefficient of polynomial fits for different materials constants (β, n, α, lnA and Q) of deformed AA7150-5 wt% B_4C composite. (Constants b_o-b_5, c_o-c_5, d_o-d_5, e_o-e_5 and f_o-f_5 correspond to Eq. (15))

β	Eq. 15 (i)	n	Eq. 15 (ii)	α	Eq. 15 (iii)	lnA	Eq. 15 (iv)	Q	Eq. 15 (v)
b_o	0.28	c_o	43.62	d_o	0.0066	e_o	44.78	f_o	279.65
b_1	− 0.2067	c_1	− 55.467	d_1	− 0.0013	e_1	− 65.207	f_1	438.2
b_2	0.4	c_2	273.68	d_2	0.0049	e_2	387.42	f_2	− 3384.1
b_3	− 0.333	c_3	− 718.42	d_3	− 0.0263	e_3	− 1215.4	f_3	10,160
b_4	2E-09	c_4	931.67	d_4	0.0583	e_4	1708.3	f_4	− 14,137
b_5	− 1E-09	c_5	− 491.67	d_5	− 0.0417	e_5	− 891.67	f_5	7558.3

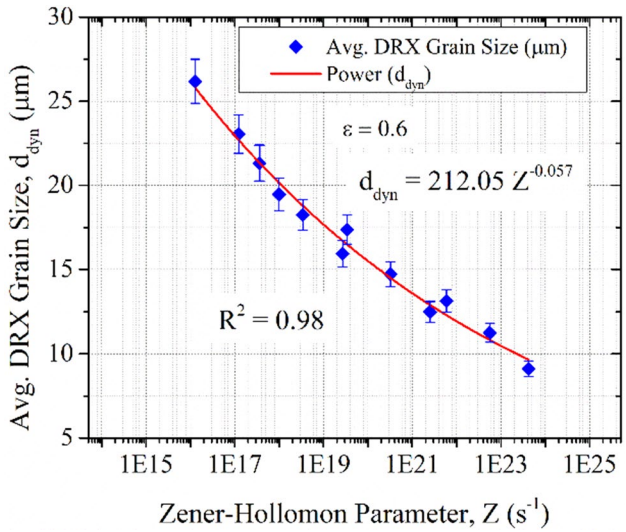

Fig. 14 Correlation between avg. DRXed grain size and Z parameter of deformed AA7150-5 wt% B_4C composite

3.4 Development of DRX Model

The DRX grain behaviour of any materials for various HD conditions can be described by using the following power-law equation [45].

$$d_{dyn} = A_{dyn} Z^{n_{dyn}} \tag{16}$$

A_{dyn} and n_{dyn} are material constants, and d_{dyn} is the dynamically recrystallized grain size. The above power-law expression can be used to predict grain size behaviour of the material for different deformation conditions. The mathematical DRX model of deformed AA7150-5 wt% B_4C composite was developed in terms of the Z parameter by fitting power-law in the formula of Eq. (16) as shown in Fig. 14. This DRX model was developed at 0.6 strain deformed specimen. The DRX models developed between grain size and Zener–Holloman parameters of deformed AA7150-5 wt% B_4C composite is expressed as follows:

$$d_{dyn} = 212.06Z^{-0.057} \quad \left(R^2 = 0.983\right) \tag{17}$$

Figure 14 represents the correlation between Z parameter and average DRXed grain size. It is seen that the DRXed grains were universally proportional to the deformation parameters [46]. The grain size of the composite was reduced with higher strain values. At lower temperature the grain sizes increased and with higher temperature, and with lower strain rate, the reasons are explained in Sect. 3.2. The Z parameter (Eq. (5)) values are decreased with higher deformation temperature and with lower strain rate, as a result the DRXed grain size is increased (Fig. 14). Contrarily, the Z parameter values are higher with lower temperature, and with higher strain rate, it indicating that the DRXed grain size decrease with increasing Z parameter. As a result of this, it could be assumed that the DRXed grains are depended entirely on the deformation conditions as demonstrated in Figs. 7 and 9. Therefore, the proposed microstructure model (Eq. 17) could be used to predict the DRXed grain size of the deformed AA7150-5 wt% B_4C composite for different deformation conditions.

3.5 Validation of Constitutive and DRX Models Deformed AA7150-5 wt% B_4C Composite

It is essential to affirm the accuracy of the proposed constitutive and DRX models for deformed AA7150-5 wt% B_4C composite. Figure 15 indicates the graph showing the relationship between experimental/measured values and predicted values of deformed AA7150-5 wt% B_4C composite for flow stress and avg. DRXed grain size. The predicted flow stresses were calculated from Eq. (7), using material constant values obtained from the constitutive model in Eq. (15). Similarly, the predicted DRXed grain sizes were calculated using a developed DRXed model for different deformation conditions and illustrated in Table 6. It is evident from Fig. 15 that the experimental/measured and predicted values are close to the line of best fit which provides evidence of the precision of proposed constitutive and DRX models. The regression coefficient (R^2) is found to be 0.93 and 0.98 for the flow stress and avg. DRXed grain size respectively, which signifies good correlation between predicted and experimental/measured data.

Further, the accuracy of the developed models and DRX models of the deformed AA7150-5 wt% B_4C composite was

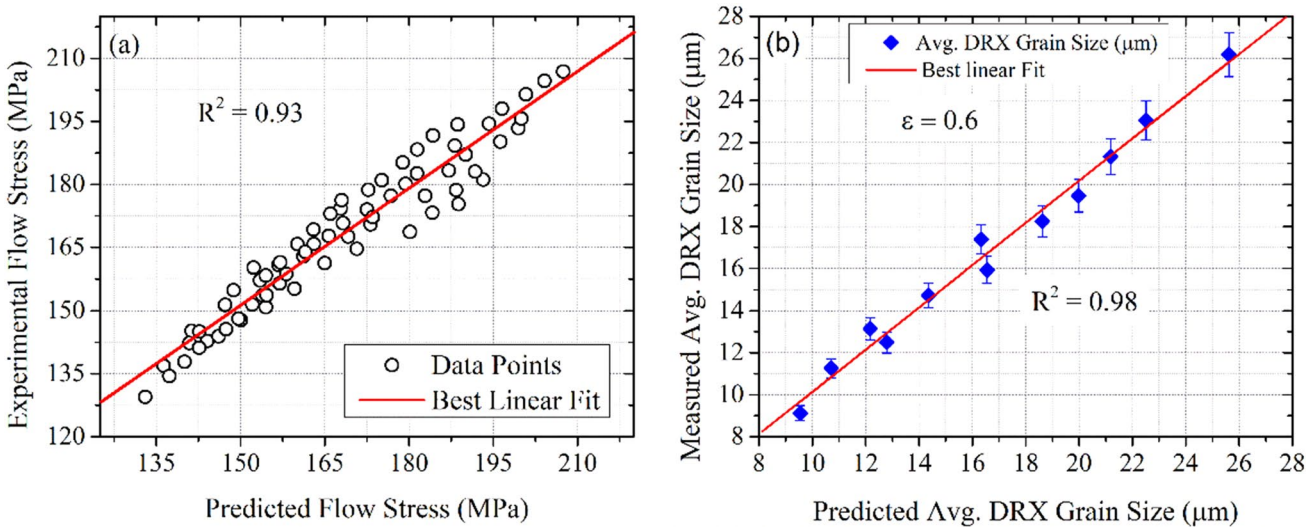

Fig. 15 Comparisons between experimental values and predicted values of deformed AA7150-5 wt% B_4C composite are **a** flow stress and **b** avg. DRXed grain size

Table 6 Correlation between measured and predicted grain size of deformed AA7150-5 wt% B_4C composite at a 0.6 strain level

Temp. (K)	$\dot{\varepsilon}$ (s^{-1})	Measured Grain size (d_m)	Predicted Grain size (d_p)	Absolute error (δ) %	Mean absolute error (δ_m) %
623	0.01	13.15	12.17	7.40	5.65
623	0.1	11.26	10.71	4.88	
623	1	9.12	9.54	4.69	
673	0.01	17.37	16.33	5.95	3.6
673	0.1	14.73	14.36	2.48	
673	1	12.49	12.78	2.36	
723	0.01	21.32	21.17	0.65	2.21
723	0.1	18.24	18.61	2.07	
723	1	15.93	16.55	3.89	
773	0.01	26.18	25.61	2.16	2.41
773	0.1	23.05	22.51	2.33	
773	1	19.46	19.99	2.72	

evaluated by determining the absolute error (δ) and mean absolute error (δ_m) between experimental/measured and predicted data. The δ error was determined by the following expression.

$$\delta = \left|\frac{\sigma_p - \sigma_e}{\sigma_e}\right| X100\% (or) \left|\frac{d_p - d_m}{d_m}\right| X100\% \quad (15)$$

where σ_p, d_p are predicted flow stress and avg. DRX grain size, respectively, σ_e = experimental flow stress and d_m = measured avg. DRX grain size.

The δ and δ_m errors determined between experimental/measured and predicted flow stress for various conditions were not exceeding 7.72% and 2.81% respectively. Similarly, the δ and δ_m errors were calculated between experimental/measured and predicted avg. DRXed grain size for different conditions at 0.6 strain level, as represented in Table 6. It is noticed that δ and δ_m errors do not exceed 7.4% and 3.47% respectively. As a result of this, overall, it is concluded that the proposed model and DRX models of deformed AA7150-5 wt% B_4C composite were precise and reliable enough to predict the flow stress and grain size.

4 Conclusions

The new AA7150-5 wt% B_4C composite was fabricated through ultrasonic-vibrated stir casting process. The hot compression test was performed on hydraulic press for various deformation temperatures (623–773 K) and strain rates (0.01–1 s^{-1}). The signification conclusions drawn are:

- The flow stress and microstructure of the AA7150-5 wt% B_4C composite were significantly altered for different deformation conditions during hot compression test. The grain size of the deformed composite was measured by LIM method, and it was found to vary from 3 to 48 μm based on different deformation conditions.
- The constitutive models were developed as a function of the strain of deformed AA7150-5 wt% B_4C composite which is used to forecast the flow stress behaviour for different deformation conditions.
- The mathematical microstructure model was developed of deformed AA7150-5 wt% B_4C composite between the avg. DRXed grain size and Z parameter. This model potential use to forecast the grain size behaviour for different deformation conditions.
- The flow stress and DRXed grain size were obtained through the constitutive and DRXed models, which were correlated with experimental results, confirming excellent agreement. The models developed are reliable enough to predict AA7150-5 wt% B_4C properties for various conditions.

Acknowledgements I would like to thank Dr. M Raja Vishwanathan, Head of Humanities & Social Science Department, National Institute of Technology, Warangal, Telangana, India, for spending valuable time to proofread the paper and for his useful suggestions.

References

1. T.B. Rao, J. Tribol. **140**, 031601 (2017)
2. M.A. Salem, I.G. El-Batanony, M. Ghanem, J. Eng. Mater. Technol. **139**, 011007 (2017)
3. R. Raj, D.G. Thakur, Materialwiss Werkstofftech **49**, 1068 (2018)
4. N. Pagidi Madhukar, C.S.P. Selvaraj, G.B. Rao, Veeresh Kumar, Compos. Part B Eng. **175**, 107136 (2019)
5. R. Miranda, University of Lisbon, Thesis, Ch.4 113 (2014)
6. G.V. Kumar, P.P. Panigrahy, S. Nithika, R. Pramod, C.S.P. Rao, Compos. Part B Eng. **175**, 107138 (2019)
7. R. Singh, R. Singh, J.S. Dureja, I. Farina, F. Fabbrocino, Compos. Part B Eng. **115**, 203 (2017)
8. A.F. Fedotov, Compos. Part B Eng. **163**, 139 (2019)
9. G. Tosun, M. Kurt, Compos. Part B Eng. **174**, 106965 (2019)
10. N. Jin, H. Zhang, Y. Han, W. Wu, J. Chen, Mater. Charact. **60**, 530 (2009)
11. P. Madhukar, N. Selvaraj, C.S.P. Rao, G.B. Veereshkumar, J. Alloy. Compd. **815**, 152464 (2020)
12. P. Madhukar, N. Selvaraj, C.S.P. Rao, G.B. Veeresh Kumar, Ceram. Int. **46**, 17103 (2020)
13. P. Madhukar, N. Selvaraj, R. Gujjala, C.S.P. Rao, Ultrason. Sonochem. **58**, 104665 (2019)
14. U.K. Annigeri, G.V. Kumar, J. Test. Eval. **47**, 4465 (2019)
15. G.E. Kodzhaspirov, M.I. Terentyev, Mater. Phys. Mech. **13**, 70 (2012)
16. M. Shaban, B. Eghbali, J. Mater. Sci. Technol. **27**, 359 (2011)
17. Y.C. Lin, S.C. Luo, L.X. Yin, J. Alloy. Compd. **739**, 590 (2018)
18. R. Seetharam, S.K. Subbu, M.J. Davidson, Metallogr. Microstruct. Anal. **70**, 176 (2018)
19. P. Qiu, H. Li, X. Sun, Y. Han, G. Huang, W. Lu, D. Zhang, J. Alloy. Compd. **699**, 874 (2017)
20. X.J. Wang, K. Wu, H.F. Zhang, W.X. Huang, H. Chang, W.M. Gan, M.Y. Zheng, D.L. Peng, Mater. Sci. Eng. A **465**, 78 (2007)
21. K.K. Deng, K. Wu, X.J. Wang, Y.W. Wu, X.S. Hu, M.Y. Zheng, W.M. Gan, H.G. Brokmeier, Mater. Sci. Eng. A **527**, 1630 (2010)
22. A. El-Sabbagha, M. Solimanb, M. Tahaa, H. Palkowski, J. Mater. Process. Technol. **212**, 497 (2012)
23. T. Sheppard, A. Jackson, Mater. Sci. Tech. **13**, 203 (1997)
24. C. Shi, W. Mao, X.-G. Chen, Mater. Sci. Eng. A **571**, 83 (2013)
25. C. Shi, X.-G. Chen, Mater. Sci. Eng. A **596**, 183 (2014)
26. C. Shi, X.-G. Chen, Mater. Sci. Eng. A **613**, 91 (2014)
27. H. Zhang, N.P. Jin, J.H. Chen, T. Nonferr. Metal. Soc. **21**, 437 (2011)
28. F. Thevenot, J. Eur. Ceram. Soc. **6**, 205 (1990)
29. D. Patidar, R.S. Rana, Mater. Today Proc. **4**, 2981 (2017)
30. R.M. Mohanty, K. Balasubramanian, Key Eng. Mater. **395**, 125 (2009)
31. R. Seetharam, S.K. Subbu, M.J. Davidson, J. Manuf. Process. **28**, 309 (2017)
32. M. Zhou, Y.C. Lin, J. Deng, Y.-Q. Jiang, Mater. Design **59**, 141 (2014)
33. H.Q. Huang, H.S. Di, N. Yan, J.C. Zhang, Y.G. Deng, R.D.K. Misra, J.P. Li, Acta Metall. Sin. Engl. **31**, 503 (2018)
34. M.R. Rokni, A. Zarei-Hanzaki, C.A. Widener, P. Changizian, J. Mater. Eng. Perform. **23**, 4002 (2014)
35. X. Xia, P. Sakaris, H.J. McQueen, Mater. Sci. Tech. **10**, 487 (1994)
36. D. Li, Q. Guo, S. Guo, H. Peng, Z. Wu, Mater. Design **32**, 696 (2011)
37. H. Zhang, K. Zhang, H. Zhou, Z. Lu, C. Zhao, X. Yang, Mater. Design **80**, 51 (2015)
38. Q.M. Guo, D.F. Li, S.L. Guo, Mater. Manuf. Process. **27**, 990 (2012)
39. X.J. Wang, X.S. Hu, K.B. Nie, K.K. Deng, K. Wu, M.Y. Zheng, Mater. Sci. Eng. A **545**, 38 (2012)
40. Y.C. Lin, X.-M. Chen, Mater. Design **32**, 1733 (2011)
41. C.M. Sellars, J. McG. Tegart, Int. Metall. Rev. **17**, 1 (1972)
42. C. Zener, J.H. Hollomon, J. Appl. Phys. **15**, 22 (1944)
43. L. Chen, G. Zhao, J. Yu, W. Zhang, Mater. Design **66**, 129 (2015)
44. W.F. Gale, T.C. Totemeier, *Smithells Metals Reference Book*, 8th edn. (Butterworth-Heinemann, Oxford, 2003)
45. T. Matsui, H. Takizawa, H. Kikuchi, S. Wakita, in *Proceedings of the 9th International Symposium on Superalloys*, ed. by T.M. Pollock, R.D. Kissinger, R.R. Bowman, K.A. Green, M. McLean, S. Olson, J.J. Schim. Superalloys 2000, Seven Springs, September 17–21 2000 (TMS, Warrendale, 2000), pp. 127–133
46. R. Seetharam, S.K. Subbu, M.J. Davidson, J. Eng. Mater. T. ASME **140**, 021003 (2018)

Publisher's note Springer Nature remains neutral with regard to jurisdictional claims in published maps and institutional affiliations.